

In conclusion, this work reports the first high resolution  $^{13}\text{C}$  NMR study of the organic superconductor  $\kappa\text{-(ET)}_2\text{-Cu[N(CS)}_2\text{]Br}$  via MAS and cross-polarization techniques with  $^{13}\text{C}$ -enriched ET molecules. The Knight shift tensor of the central carbon atoms has been derived. A lowering of the symmetry below 273 K has been deduced from the splitting of the  $^{13}\text{C}$  MAS NMR lines of the central carbons. A distortion of the organic lattice occurs below about 200 K when the motion of the ethylene groups is frozen. The incommensurate character of the distortion is implied by the inhomogeneous broadening of the NMR lines. This feature rules out the commensurate nature claimed from earlier diffuse X-ray scattering experiments.

Received: September 11, 1997  
Final version: March 6, 1998

- [1] T. Ishiguro, K. Yamaji, *Organic Superconductors*, Springer, Berlin **1990**.
- [2] J. Williams, *Science* **1991**, 252, 1501.
- [3] A. M. Kini, U. Geiser, H. H. Wang, K. D. Carlson, J. M. Williams, W. K. Kwok, K. G. Vandervoort, J. E. Thompson, D. L. Stupka, D. Jung, M. H. Whangbo, *Inorg. Chem.* **1990**, 29, 2555.
- [4] D. Jérôme, *Science* **1991**, 252, 1509.
- [5] U. Geiser, A. Kini, H. Wang, M. Beno, J. Williams, *Acta Crystallogr. C* **1991**, 47, 190.
- [6] U. Geiser, A. M. Kini, H. H. Wang, M. A. Beno, J. M. Williams, *Physica C* **1991**, 174, 475.
- [7] Y. Nogami, J. Pouget, H. Ito, T. Ishiguro, G. Saito, *Solid State Commun.* **1994**, 89, 113.
- [8] H. Mayaffre, *Ph.D. Thesis*, Université Paris XI, **1996**.
- [9] P. Wzietek, H. Mayaffre, D. Jérôme, S. Brazovskii, *J. Phys. I (Paris)* **1996**, 6, 2011.
- [10] H. Mayaffre, P. Wzietek, D. Jérôme, C. Lenoir, P. Batail, *Europhys. Lett.* **1994**, 28, 205.
- [11] S. D. Soto, C. Slichter, H. Wang, U. Geiser, J. Williams, *Phys. Rev. Lett.* **1993**, 70, 2956.
- [12] J. Larsen, C. Lenoir, *Org. Synth.* **1993**, 256.
- [13] M. Mehring, *High Resolution NMR in Solids*, Springer, Berlin **1983**.
- [14] J. Herzfeld, A. Berger, *J. Chem. Phys.* **1980**, 73, 6021.
- [15] T. Klutz, I. Hennig, U. Haerberlen, D. Schweitzer, *Appl. Magn. Res.* **1991**, 2, 441.
- [16] S. D. Soto, C. Slichter, A. Kini, H. Wang, U. Geiser, J. Williams, *Phys. Rev. B* **1995**, 52, 10 364.
- [17] A. Kawamoto, K. Miyagawa, Y. Nakazawa, K. Kanoda, *Phys. Rev. Lett.* **1995**, 74, 3455.
- [18] A. Vainrub, private communication.
- [19] F. Artzner, private communication.
- [20] T. Emge, P. Leung, M. Beno, A. Schultz, H. Wang, L. Sowa, J. Williams, *Phys. Rev. B* **1984**, 30, 6780.
- [21] A. Vainrub, S. Vija, E. Lippma, V. Prigodin, R. Beha, M. Mehring, *Phys. Rev. Lett.* **1992**, 69, 3116.
- [22] A. Vainrub, I. Kheinmaa, E. Yagubskii, *JETP Lett.* **1987**, 44, 317.

## Fabrication of Magnetic Spider Silk and Other Silk-Fiber Composites Using Inorganic Nanoparticles\*\*

By Eric L. Mayes, Fritz Vollrath, and Stephen Mann\*

Spider dragline silk is a semicrystalline biopolymer with a unique combination of high tensile strength, high elasticity, and high modulus. The 0.2 to 10  $\mu\text{m}$  diameter silk fibers have a higher breaking energy than other natural or synthetic fibrous polymers, far exceeding that of high tensile steel and Kevlar on a weight-for-weight basis.<sup>[1]</sup> Thus, silk fibers could have important applications in impact-proof textiles or other structural fabrics where strong, flexible materials are desirable. Moreover, the inherent biocompatibility of silk could be exploited in the preparation of new strong biomaterials for use in artificial tendons or non-allergenic sutures.<sup>[2]</sup> A further possibility might be to modify the properties of silk fibers by integration with those of other materials to give functionalized hybrid composites with enhanced or entirely new applications. For example, cross-linking of dragline silk fibers with organic polymeric precursors produces an apparent improvement in the tensile strength.<sup>[3]</sup>

Although silk is a highly hydrophobic, insoluble biopolymer, it has recently been shown that dragline spider silk can undergo a reversible transformation to a supercontracted state when placed in water or polar organic solvents.<sup>[4]</sup> These observations suggest a possible general route to the functionalization of silk fibers by aqueous-based interactions with the modified supercontracted state. In this paper we describe a specific approach in which hybrid silk materials are prepared by binding inorganic nanoparticles to the surface and near-surface regions of silk fibers immersed into colloidal sols.

Our main focus has been on the fabrication of magnetic spider silk fibers. Bundles of ca. 200 individual silk fibers were prepared by cutting 3 cm lengths of dragline spider silk from a continuous spool produced by *Nephila edulis*. We used dragline silk originating from the Major Ampullate glands, and the threads were drawn mechanically from immobilized but fully awake spiders at a speed of 2 cm/s onto either 1 cm diameter glass tubes or photographic slide frames. These bundles were suspended by tweezers and

[\*] Prof. S. Mann, E. L. Mayes  
Department of Chemistry, University of Bath  
Bath BA2 7AY (UK)  
Prof. F. Vollrath  
Department of Zoology  
Universitetsparken B135, DK-8000 Aarhus (Denmark)

[\*\*] We thank Dr. T. Kearney and Dr. D. Goddard of BNFL plc for support of a postgraduate studentship to ELM, Dr. S. L. Burkett for preparation of the hydrophobic gold colloid, H. B. Joergensen for the preparation of dragline silk fibers, and Dr. Z. Shao for setting up and calibrating the mechanical gauge.

mechanically lowered into either a water or water/methanol sol of 10 to 20 nm diameter superparamagnetic magnetite ( $\text{Fe}_3\text{O}_4$ ) particles for 2 min. Alternatively, single fibers, mounted across a twin-pronged variable caliper,<sup>[5]</sup> were mechanically submerged into the nanocolloidal suspensions. After submersion, the fibers were slowly withdrawn from the colloidal sol and allowed to dry in air at ambient temperatures. The resulting dark brown fibers were coated with a dense coherent film of the magnetite nanocrystallites (Figs. 1A and B). High magnification images (e.g., Fig. 1C) showed that the magnetite–silk composites displayed some surface roughness, indicating that the thickness of the mineral films was substantial. The mineralized fibers, however, retained their natural flexibility without significant disruption of the magnetite coating (Fig. 1D). Moreover, the combination of intrinsic mechanical and fabricated magnetic properties enabled dried fibers to be oriented in the presence of an external magnetic field because fibers suspended against gravity tracked the position of a strong magnet. This was observed by fixing the fibers with tweezers in the presence of a 1.5 cm diameter neodymium–iron–boron slug (Fig. 2).

Mineralized fibers were embedded in epoxy resin and thin-sectioned for scanning electron microscopy (SEM) and energy dispersive X-ray (EDX) analysis studies using a JEOL 6310 SEM operating at 20 kV. The intensity of the iron  $K\alpha$  peak was determined for four different cross-sections of each sample. EDX analysis of sectioned magnetite–silk fibers showed high intensities for the iron  $K\alpha$  absorption around and possibly within the surface regions of the composites (Fig. 3). Analysis of the iron  $K\alpha$  peak intensities of cross-sectioned fibers showed that similar iron adherence was achieved for composites prepared from water or water/methanol solvents. Samples that were extensively washed in water or water/methanol for 2 min remained

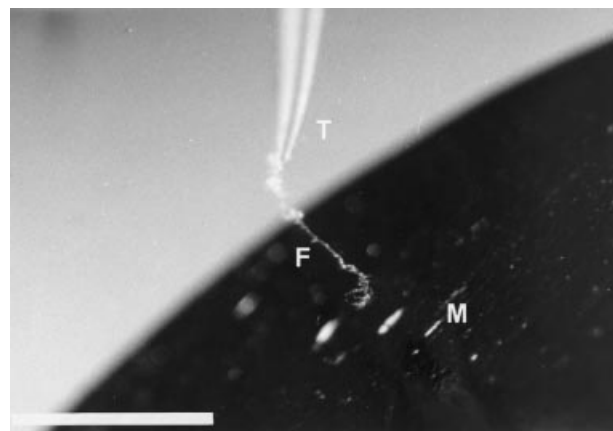


Fig. 2. Optical image illustrating magnetic attraction of a magnetite–silk fiber (F) to an external magnet (M). The fiber is held at the end of a vertically aligned pair of tweezers (T). Scale bar = 5 mm.

dark brown in color but had reduced iron contents as shown by EDX analysis of cross-sectioned material; similar observations were made for magnetite–silk fibers that had been sonicated for 1 h in water or water/methanol mixtures.

Stress–strain gauge measurements on individual magnetite–silk fibers showed negligible differences between the mechanical properties of the composite materials and unmineralized spider silk fibers (Fig. 4). The stress–strain properties determined from the breaking strength measurements were typical of natural silk (Table 1).<sup>[3]</sup> The breaking strengths were similar regardless of coating or solvent used in the preparations, but slight differences existed in the initial modulus and breaking elongation. The fibers exposed to water showed a slightly higher initial modulus, whereas the fibers prepared from methanol/water mixtures had a slightly higher breaking elongation. These mechani-

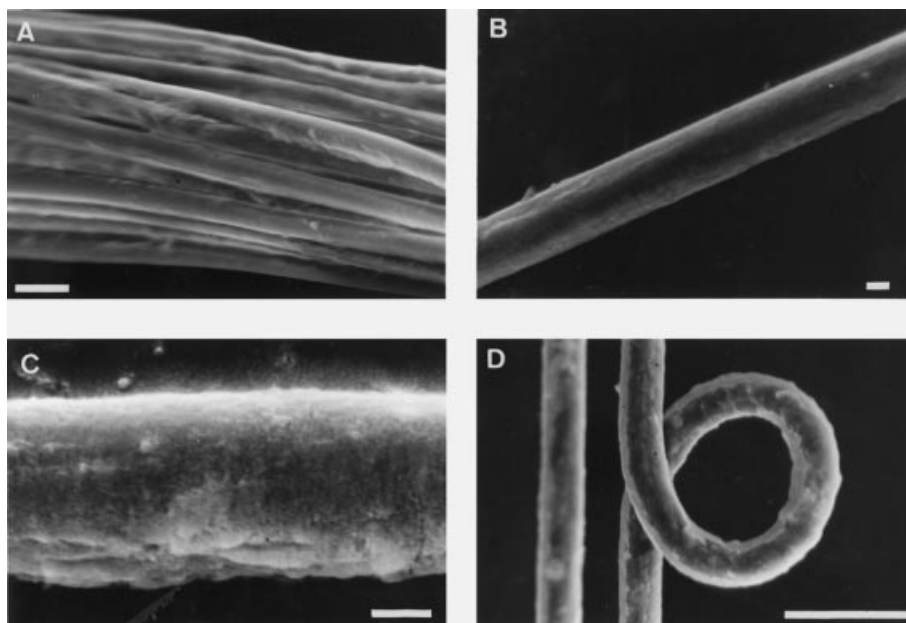


Fig. 1. SEM images of magnetite-coated silk fibers. A) Low magnification image showing bundle of magnetite-coated spider silk fibers, scale bar = 10  $\mu\text{m}$ . B) Individual silk fiber with magnetite surface film, scale bar = 1  $\mu\text{m}$ . C) Higher magnification image showing surface texture of the magnetite layer, scale bar = 1  $\mu\text{m}$ . D) Magnetite–silk fiber displaying retained flexibility without significant loss of the mineral phase, scale bar = 10  $\mu\text{m}$ .

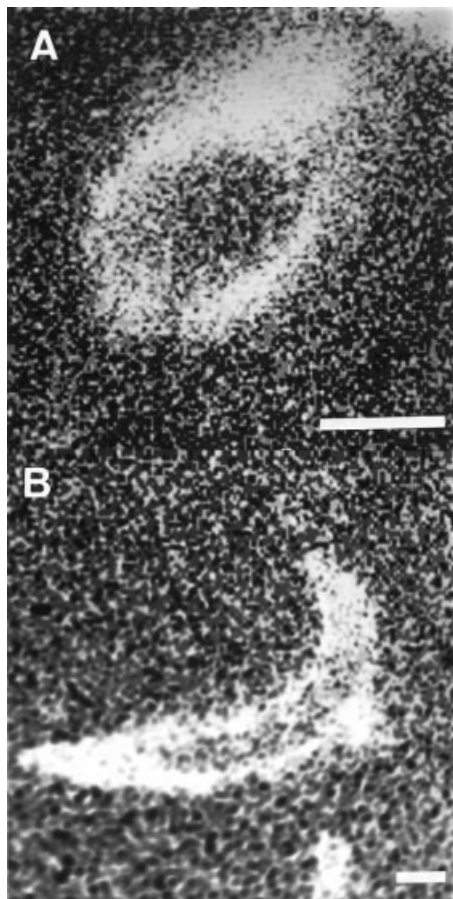


Fig. 3. Energy dispersive X-ray spatial mapping images for iron in magnetite-silk fibers sectioned A) approximately perpendicular to and B) oblique to the fiber axis. Scale bar = 1  $\mu\text{m}$  in both images.

cal properties were consistent with recent studies of *Ara-neus diadematus* dragline silk exposed to different solvents.<sup>[4]</sup>

We also prepared inorganic-silk fibers from colloids consisting of hydrophobic nanoparticles. Bundles of fibers, as well as individual fibers mounted on twin-pronged calipers, were submerged for 2 min in a 2-propanol sol of 2 nm gold particles that were surface-functionalized with 4-mercapto-phenol.<sup>[6]</sup> Air drying of the dipped samples produced dark purple fibers with uniform and stable metal coatings (Fig. 5A). The gold coating was particularly resilient to subsequent washings with water and sonication. A similar procedure was used for the fabrication of inorganic-silk fibers coated in hydrophobic 5 nm diameter particles of cadmium sulfide. The semiconductor particles were prepared by chemical precipitation in reverse micelles formed from heptane/water/surfactant mixtures. Immersion of silk fibers into these dispersions produced pale white mineralized fibers that were covered in a homogeneous coating of CdS (Fig. 5B). The mechanical properties of both the Au- and CdS-coated silk fibers were essentially the same as determined for the unmodified silk (Table 1).

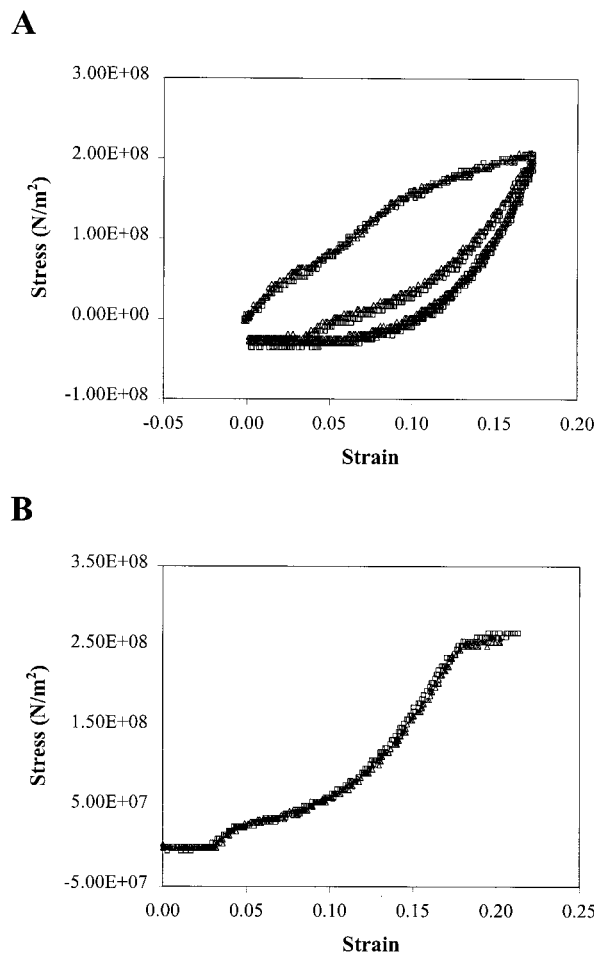


Fig. 4. Stress-strain curves for a control (unmodified) silk fiber (triangles) and magnetite-coated silk fiber (squares) showing A) hysteresis and B) breaking points.

Table 1. Mechanical properties of *Nephila edulis* dragline silk-magnetite composites.

	Initial modulus [ $\times 10^9 \text{ N/m}^2$ ]	Breaking strength [ $\times 10^8 \text{ N/m}^2$ ]	Breaking elongation [%]
Control bare silk	1.1 $\pm$ 0.1	2.5 $\pm$ 0.1	22 $\pm$ 2.0
Magnetite (H <sub>2</sub> O)	1.5 $\pm$ 0.2	2.2 $\pm$ 0.3	18 $\pm$ 2.0
Magnetite (CH <sub>3</sub> OH/H <sub>2</sub> O)	1.1 $\pm$ 0.1	2.3 $\pm$ 0.2	28 $\pm$ 1.0
Gold	1.2 $\pm$ 0.3	2.8 $\pm$ 0.1	25 $\pm$ 7.0
Cadmium sulfide	1.4 $\pm$ 0.3	2.2 $\pm$ 0.4	19 $\pm$ 2.0
Silica	1.9 $\pm$ 0.5	2.9 $\pm$ 0.3	22 $\pm$ 5.0

Finally, we prepared silk fibers coated in the electroconducting polymer polypyrrole by a two-step procedure involving Fe<sup>III</sup>-catalyzed oxidative polymerization. Iron-coated fibers were prepared by dipping fibers in a 1 M FeCl<sub>3</sub> solution for 30 min and air-drying overnight. The resulting fibers were brown in color due to the formation of an iron oxide surface coating during drying of the Fe<sup>III</sup> salt solution. The mounted fibers were then submerged in pyrrole for 2 min, removed, and rinsed with water to quench polymerization. After drying in air, dark greenish-black fibers coated in polypyrrole were produced (Fig. 5C). Although the Fe<sup>III</sup> layer appeared to be stable, the polymer coating

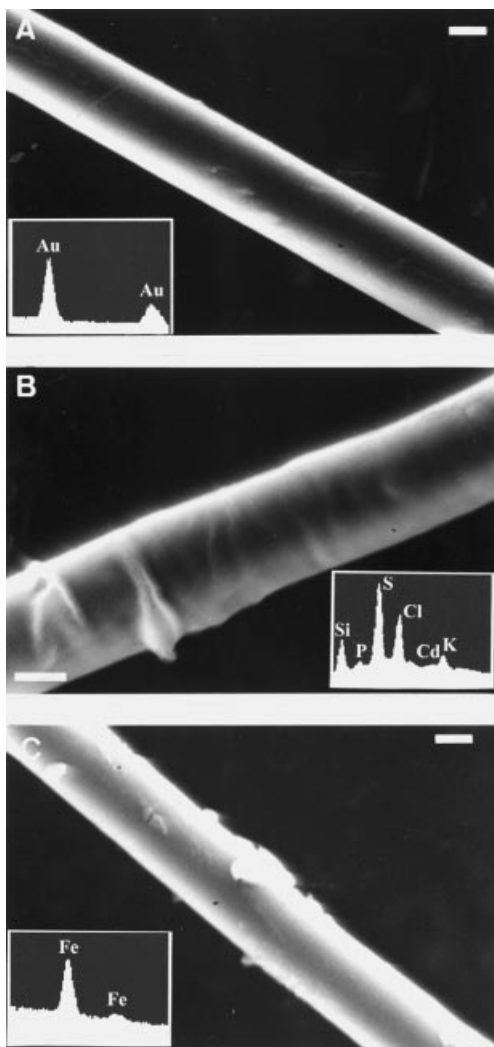


Fig. 5. SEM images and corresponding EDX analysis spectra for silk fiber composites prepared with nanoparticle coatings of A) hydrophobic gold, B) surfactant-coated CdS, and C) polypyrrole. Scale bars = 1  $\mu\text{m}$  in all micrographs.

could be partially removed by sonication or mechanical flexing.

Our results indicate that mineral-coated silk fibers can be readily produced by a straightforward approach using nanoparticle suspensions. The method is versatile, easy to perform, and environmentally benign, suggesting that a wide range of silk-fiber hybrids could be routinely fabricated by this approach. At first sight, the use of dragline spider silk as a fibrous template for the adsorption and consolidation of thin films of magnetite nanoparticles is somewhat surprising, as the hydrophobic nature of the biopolymer should be incompatible with the charged and hydrated nature of the iron oxide surfaces. Indeed, use of hydrophobic nanoparticles, such as ligand-capped Au or surfactant-encapsulated CdS clusters, dispersed in organic solvents improved the wetting and mechanical stability of the inorganic coatings. It remains the case, however, that the mag-

netite coatings were well-defined and relatively stable when adsorbed from aqueous solutions. One possibility is that there are hydrogen bonding interactions at the oxide–silk interface. Recent observations have shown that immersion of spider silk fibers in water and other polar solvents induces reversible structural changes, consistent with hydrogen bonding networks within the near-surface structure of the silk.<sup>[4]</sup> In principle, oxo and hydroxyl species on the mineral surface could bind to polar amino acids that are exposed by interaction with solvent molecules. The collective outcome of such processes will be dependent on the binding site density and this is probably enhanced by the small size of the oxide nanoparticles, which generates a relatively large number of polar surface sites owing to the high surface area to volume ratio. Moreover, the small dimensions appear to be important for determining the structural integrity of the coatings, presumably because the nanoparticles give rise to close packed and highly consolidated aggregates during drying. In contrast, coatings prepared from aqueous suspensions of sub-micrometer size particles, such as colloidal silica, were extremely friable and flaked off the silk fibers during manipulation of the sample (data not shown). Similar considerations were discussed for nanocolloids used for the fabrication of ordered silica macrostructures within bacterial templates.<sup>[7]</sup>

Silk-fiber materials that combine the natural strength and elasticity of the biopolymer with physical properties such as magnetism, electrical conductivity, or semiconductivity might be useful as smart structural fabrics in a range of applications. Silk composites with magnetic properties, for example, could be integrated into devices concerned with audio reproduction where strong fabrics that respond to a magnetic field are required. We plan to continue to explore this system with the use of hydrophobic magnetic materials to achieve uniform coatings with high magnetization. Recently, evidence of an interesting hierarchical tube/core microstructure within the dragline silk has been reported,<sup>[8]</sup> suggesting that these micro-architectures could be used in future work to integrate inorganic components within silk fibers to produce biopolymer composites with significantly increased mineral loadings.

## Experimental

A colloidal magnetite ( $\text{Fe}_3\text{O}_4$ ) sol was prepared according to a previously reported procedure [9] by dropwise addition of 50 mL of 1 M  $\text{Me}_4\text{-NOH}\cdot 5\text{H}_2\text{O}$  to a stirred mixture of 2.1 M  $\text{FeCl}_3\cdot 6\text{H}_2\text{O}$  (2.3 g in 4 mL  $\text{H}_2\text{O}$ ) and 6.0 M  $\text{Fe}(\text{NH}_4)_2(\text{SO}_4)_2$  (1.69 g in 1 mL of 2 M HCl). The resulting black sol was stirred at room temperature for 1 h, then sonicated in a water bath for 1 h, and finally centrifuged at 20000 rpm for 2 h. The supernatant was decanted and the pellet resuspended in  $\text{H}_2\text{O}$  by sonication. The centrifugation and washing procedures were repeated and the resuspended sol was filtered through a 13 mm diameter, 0.2  $\mu\text{m}$  cellulose nitrate membrane. The final colloidal solution had a pH of 9.3. The negatively charged magnetite nanocolloid was used as a suspension either in water or in a 1:1 methanol/water mixture.

A nanocolloidal cadmium sulfide (CdS) sol was prepared in reverse micelles according to a previously reported procedure [10]. Reverse micelles were prepared by dissolving 1.67 g of AOT surfactant in 65 mL of heptane,

followed by dropwise addition of 338  $\mu\text{L}$  of  $\text{H}_2\text{O}$  while stirring vigorously. The homogeneous mixture was purged with nitrogen and 5  $\mu\text{L}$  of 1 M  $\text{Cd}(\text{NO}_3)_2 \cdot 4\text{H}_2\text{O}$  was then added via a microliter syringe to 10 mL of the stirred reverse micelle solution. 5  $\mu\text{L}$  of 1 M  $\text{Na}_2\text{S}$  was slowly added and the solution was stirred for 20 min. Particle sizes were determined by UV-vis spectroscopy.

Mechanical testing was performed on single fibers of the inorganic-silk composites, which were attached to the twin arms of a custom-built stress-strain gauge using cyanoacrylate adhesive, and hysteresis cycles and breaking strength measurements were performed at ambient conditions of 29 °C and 34 % relative humidity. The measured stress was normalized using fiber diameters determined by SEM (mean diameter =  $3.1 \pm 0.5 \mu\text{m}$ ). The custom stress-strain gauge consisted of a FORT 10 force transducer (World Precision Instruments) and a Pen Motor Assembly (Hewlett Packard).

Received: December 1, 1997

- [1] J. M. Gosline, M. E. DeMont, M. W. Denny, *Endeavour* **1986**, *10*, 37.
- [2] M. A. Colgin, R. V. Lewis, *Chem. Ind.* **1995**, *12*, 1009.
- [3] D. L. Dunaway, B. L. Thiel, C. Viney, *J. Appl. Polym. Sci.* **1995**, *58*, 675.
- [4] Z. Shao, F. Vollrath, *Inst. Mater. (London)* **1997**, 262.
- [5] T. Kohler, F. Vollrath, *J. Exp. Zool.* **1995**, *271*, 1.
- [6] M. Brust, J. Fink, D. Bethell, D. J. Schiffrin, C. Kiely, *J. Chem. Soc., Chem. Commun.* **1995**, *16*, 1655.
- [7] S. A. Davis, S. L. Burkett, N. H. Mendelson, S. Mann, *Nature* **1997**, *385*, 420.
- [8] F. Vollrath, T. Holtet, H. C. Thøgersen, S. Frische, *Proc. R. Soc. London B* **1996**, *263*, 147.
- [9] R. Massart, *IEEE Trans. Magn.* **1981**, *17*, 1247.
- [10] R. R. Chandler, S. R. Bigham, J. L. Coffey, *J. Chem. Educ.* **1993**, *70*, A7.

## Rapid, Solid-State Metathesis Routes to Metal Carbides\*\*

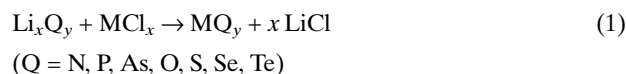
By Artur M. Nartowski, Ivan P. Parkin,\* Alan J. Craven, and Maureen MacKenzie

Transition metal carbides are inert, hard, refractory, conducting ceramics that find widespread usage in industry as components of cutting tools, crucibles, and catalysts.<sup>[1]</sup> They also play a crucial role in the formation and properties of hard steels.<sup>[2]</sup> Transition metal carbides are conventionally made by combination of the elements at elevated temperatures (>1500 °C) for extended time periods. For example, commercial grade WC used in abrasive pastes is synthesized at 2800 °C from the elements under a hydrogen atmosphere.<sup>[3]</sup> Molecular precursor routes to metal carbides have been developed in which the chemistry of the precursor decomposition has been tailored by introducing a molecular "Achilles heel" to promote carbide formation.<sup>[4,5]</sup>

[\*] Dr. I. P. Parkin, A. M. Nartowski  
Department of Chemistry  
University College London  
20 Gordon Street, London WC1H 0AJ (UK)  
Dr. A. J. Craven, Dr. M. MacKenzie  
Department of Physics and Astronomy  
University of Glasgow  
Glasgow G12 8QQ (UK)

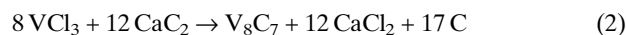
[\*\*] The authors thank the EPSRC for grants GR/L06850 and GR/K93600.

We have been interested in finding straightforward, quick, low external energy routes to inorganic materials.<sup>[6]</sup> Kaner and co-workers first reported a new method of synthesizing inorganic materials by a solid-state metathesis (SSM) reaction<sup>[7]</sup> (Eq. 1).

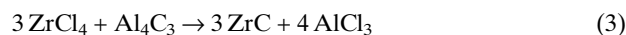


In this communication we report the first solid-state metathesis reactions for the formation of transition metal carbides via a fast (10 s), single-step reaction.

Thermal initiation of a mixture of calcium carbide with anhydrous metal chloride inside an evacuated ampoule either at the melting point of the halide or at 450 °C produces a transient red melt that, on cooling, forms a black solid with some calcium chloride layered on the surface (within 2–10 s). Trituration of the solid with methanol and water removes the coproduced calcium chloride and leaves a black or gray transition metal carbide that does not require any further annealing to induce crystallinity. In such reactions, carbon is coproduced, as shown for the reaction of  $\text{VCl}_3$  and  $\text{CaC}_2$  in Equation 2. This coproduced carbon was not detected in the triturated carbide product (by scanning electron microscopy (SEM), microanalysis, or X-ray diffraction (XRD)) and detailed inspection of the ampoule reveals that the carbon has phase separated from the vanadium carbide as a black layer on top of the coproduced  $\text{CaCl}_2$ .



An alternative carbiding reagent,  $\text{Al}_4\text{C}_3$ , was also investigated. Its reactions with transition metal halides were not as exothermic as those of  $\text{CaC}_2$  but, after annealing for 2–3 days at 800–1000 °C, always resulted in the formation of phase-pure, crystalline carbides of transition metals. Here the reactions were again promoted by the melting of the transition metal halide. When the reactions were performed inside evacuated ampoules under a temperature gradient, the coproduced aluminum halide sublimed out from the carbide product (Eq. 3).



The products were identified by X-ray powder diffraction (Table 1, Figs. 1a and b). The same single phase carbide products—stoichiometric ZrC, TiC, and WC and substoichiometric  $\text{V}_8\text{C}_7$  and  $\text{Mo}_2\text{C}$ —were obtained for both the  $\text{CaC}_2$  and  $\text{Al}_4\text{C}_3$  reactions. An exception, however, was noted for the reactions of  $\text{WCl}_4$  and  $\text{MoCl}_3$  with  $\text{CaC}_2$ . These showed some  $\text{W}_2\text{C}$  and Mo as minor second phases in addition to the principal phases WC and  $\text{Mo}_2\text{C}$ . The metal carbides were indexed (Table 1) and showed good agreement with previous literature measurements.<sup>[3]</sup> Crystallite sizes as assessed by X-ray line broadening were of the or-